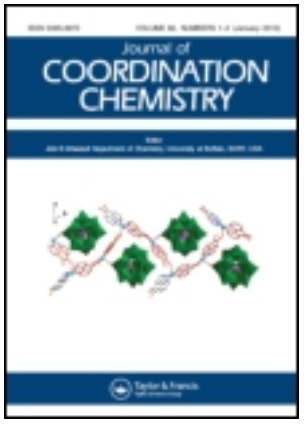

Journal of Coordination Chemistry
Publication details, including instructions for authors and subscription information:
http://www.tandfonline.com/loi/gcoo20

Tuning the oxidation states of copper ions (+I/+II) to construct different Keggin-based topology structures

Ai-Xiang Tian [a], Xiao-Ling Lin [a], Yu-Jing Liu [a], Gui-Ying Liu [b], Jun Ying [a], Xiu-Li Wang [a] & Hong-Yan Lin [a]

[a] Department of Chemistry, Bohai University, Jinzhou 121000, P.R. China

[b] Liaoning Ocean and Fisheries Science Research Institute, DaLian 116023, P.R. China

Accepted author version posted online: 04 May 2012.Published online: 17 May 2012.

To cite this article: Ai-Xiang Tian, Xiao-Ling Lin, Yu-Jing Liu, Gui-Ying Liu, Jun Ying, Xiu-Li Wang & Hong-Yan Lin (2012) Tuning the oxidation states of copper ions (+I/+II) to construct different Keggin-based topology structures, Journal of Coordination Chemistry, 65:12, 2147-2158, DOI: 10.1080/00958972.2012.688962

To link to this article: http://dx.doi.org/10.1080/00958972.2012.688962

Journal of Coordination Chemistry
Vol. 65, No. 12, 20 June 2012, 2147–2158

Tuning the oxidation states of copper ions (+I/+II) to construct different Keggin-based topology structures

AI-XIANG TIAN*†, XIAO-LING LIN†, YU-JING LIU†, GUI-YING LIU‡, JUN YING†, XIU-LI WANG† and HONG-YAN LIN†

†Department of Chemistry, Bohai University, Jinzhou 121000, P.R. China
‡Liaoning Ocean and Fisheries Science Research Institute, DaLian 116023, P.R. China

(*Received 31 January 2012; in final form 20 March 2012*)

Through tuning the oxidation states of $Cu^{I/II}$, two Keggin-based compounds with different topologies, $[Cu^{I}_{5}(btx)_4(PW^{VI}_{10}W^{V}_{2}O_{40})]$ (**1**) and $[Cu^{II}_{2}(btx)_4(SiW_{12}O_{40})]$ (**2**) (btx = 1,6-bis(1,2,4-triazol-1-yl)hexane), were synthesized and structurally characterized. In **1**, there exist decanuclear Cu^{I} circuits, which are linked through N1-containing btx ligands to construct a grid-like 2-D layer. Three sets of these layers interpenetrate to build a three-fold interpenetrating framework. The Keggin polyanions connect the adjacent three-fold interpenetrating frameworks to construct a 3-D structure. In **2**, the Cu^{II}-btx moiety shows a (6^6) 3-D hexagonal channel-style framework. The Keggin polyanion offering four terminal oxygen atoms incorporates with this metal–organic framework imbedding the channels. The different oxidation states of copper ions (+I/+II) induces distinct coordination modes of btx and Keggin polyanions and affects the whole structural topologies. Tuning the oxidation states of copper ions is an effective strategy for obtaining POM-based topologies. In addition, the electrochemical properties of **1** and **2** bulk-modified carbon-paste electrodes are reported.

Keywords: Polyoxometalate; Topology; Oxidation states; Hydrothermal synthesis; Electrochemical properties

1. Introduction

Polyoxometalates (POMs) have diversity of structures [1–3] and properties, such as in catalysis, magnetism, materials science, ion exchange, photochemical or electrochemical activity [4–6]. Interest on POMs has been on design and syntheses of discrete new types of POMs, such as multisubstituted- [7, 8] and sandwich-type [9, 10], which exhibit magnetic and catalytic applications. However, synthetic conditions are relatively rigorous in aqueous solutions. The other main development of POMs was introduction of transition metal complexes (TMCs) for modifying POMs to construct high-dimensional frameworks, synthesized under hydrothermal conditions [11–13] and a series of Keggin-based structures modified by TMCs have been obtained [14–18]. Owing to the simplicity and convenience of the hydrothermal technique, it has become

*Corresponding author. Email: tianax717@163.com

ISSN 0095-8972 print/ISSN 1029-0389 online
http://dx.doi.org/10.1080/00958972.2012.688962

popular for exploring TMC-modified POMs [19]. Selection of proper TMC modifiers is very important for forming this series, especially for choosing proper organic moieties. In previous works, rigid organic ligands, such as 2,2′-bipyridine [20] and 4,4′-bipyridine [21], built low-dimensional structures. Organic ligands [22–25], which can exhibit flexibility, are a necessary extension. In this work, we choose a flexible bis(triazole) 1,6-bis(1,2,4-triazol-1-y1)hexane (btx, scheme 1). The spacer $-(CH_2)_6-$ can bend and rotate easily to conform to the coordination environments of TM ions and POMs. The introduction of $-(CH_2)_6-$ spacer may increase the probability for construction of high-dimensional frameworks and the four potential N donors can enhance the coordination ability of btx, inducing new TMCs. Therefore, the btx ligand may construct new POM-based structures.

Many factors can affect the final structures, such as pH, temperature, and reactants [26], and exploring synthetic rules under hydrothermal conditions is attractive for target syntheses. Previous works reported the influences of different pH and reactants [27, 28]. In this work, we explore whether different oxidation states of the same TM ions can induce distinct POM-based frameworks. We chose copper ions as reactants, which can show two oxidation states (+I/+II).

Herein, we report two Keggin-based compounds with different topologies, $[Cu^{I}_{5}(btx)_4(PW^{II}_{10}W^{V}_{2}O_{40})]$ (**1**) and $[Cu^{II}_{2}(btx)_4(SiW_{12}O_{40})]$ (**2**) (btx = 1,6-bis(1,2,4-triazol-1-y1)hexane), through tuning the oxidation states of $Cu^{I/II}$ ions. The influence of different oxidation states of copper ions on structures is discussed.

2. Experimental

2.1. *Materials and methods*

All reagents and solvents for syntheses were purchased from commercial sources and used as received. Elemental analyses (C, H, and N) were performed on a Perkin-Elmer 2400 CHN elemental analyzer. Infrared (IR) spectra were obtained on an Alpha Centaurt FT-IR spectrometer with KBr pellets from 400 cm^{-1} to 4000 cm^{-1}. Thermal gravimetric analyses (TGA) were carried out in N_2 on a Perkin-Elmer DTA 1700 differential thermal analyzer with a heating rate of 10°C min^{-1}. Electrochemical measurements were performed with a CHI 660 electrochemical workstation. A conventional three-electrode system was used; Ag/AgCl (3 mol L^{-1} KCl) electrode was used as a reference electrode, a Pt wire as a counter electrode, and chemically bulk-modified carbon-paste electrodes (CPEs) as the working electrodes.

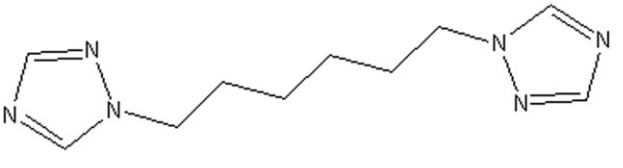

Scheme 1. The 1,6-bis(1,2,4-triazol-1-y1)hexane (btx) used in **1** and **2**.

2.2. *Preparation of the compounds*

Synthesis of $[Cu_5^{I}(btx)_4(PW_{10}^{VI}W_2^{V}O_{40})]$ (**1**). A mixture of $H_3[PW_{12}O_{40}]\cdot 12H_2O$ (0.28 g, 0.09 m mol), $Cu(CH_3COO)_2\cdot 2H_2O$ (0.33 g, 1.5 m mol), and btx (0.066 g, 0.3 m mol) was dissolved in 10 mL distilled water at room temperature. When the pH of the mixture was adjusted to 4.5 with 1.0 mol L^{-1} HCl, the suspension was put into a Teflon-lined autoclave and kept under autogenous pressure at 160°C for 3 days. After slowly cooling to room temperature, black block crystals were filtered and washed with distilled water (30% yield based on W). Anal. Calcd for $C_{40}H_{64}Cu_5N_{24}O_{40}PW_{12}$ (4076) (%): C, 11.79; H, 1.58; N, 8.25. Found (%): C, 11.73; H, 1.61; N, 8.21. IR (solid KBr pellet, cm^{-1}): 3435 (s), 3119 (w), 2925 (w), 1745 (w),1654 (s), 1537 (m), 1454 (w), 1370 (w), 1298 (w), 1142 (w), 1065 (s), 962 (s), 878 (s), 795(s).

Synthesis of $[Cu_2^{II}(btx)_4(SiW_{12}O_{40})]$ (**2**). A mixture of $H_4[SiW_{12}O_{40}]\cdot 14H_2O$ (0.31 g, 0.1 m mol), $Cu(CH_3COO)_2\cdot 2H_2O$ (0.51 g, 2.3 m mol), and btx (0.022 g, 0.15 m mol) was dissolved in 10 mL distilled water at room temperature. When the pH of the mixture was adjusted to 4.2 with 1.0 mol L^{-1} HCl, the suspension was put into a Teflon-lined autoclave and kept under autogenous pressure at 160°C for 3 days. After slowly cooling to room temperature, blue block crystals were filtered and washed with distilled water (30% yield based on W). Anal. Calcd for $C_{40}H_{64}Cu_2N_{24}O_{40}SiW_{12}$ (3882) (%): C, 12.37; H, 1.66; N, 8.66. Found(%): C, 12.43; H, 1.70; N, 8.62. IR (solid KBr pellet, cm^{-1}): 3726 (s), 3625 (s), 3106 (w), 2912 (w), 1738 (w),1693 (m), 1521 (s), 1454 (w), 1356 (w), 1280 (m), 1124 (s), 968 (w), 923 (s), 872 (w), 792 (s), 673 (s).

2.3. *X-ray crystallographic study*

X-ray diffraction analysis data for **1** and **2** were collected on a Bruker Smart Apex CCD diffractometer with Mo-Kα radiation ($\lambda = 0.71073$ Å) at 293 K. The structures were refined by full-matrix least-squares on F^2 using the SHELXTL crystallographic software package [29]. All hydrogen atoms attached to carbon were generated geometrically. The crystal and structure refinement data for **1** and **2** are summarized in table 1. Selected bond lengths (Å), angles (°), and symmetry codes of **1** and **2** are listed in table 2.

2.4. *Preparation of 1- and 2-CPEs*

Compound **1** modified CPE (**1**-CPE) was fabricated as follows: 90 mg of graphite powder and 8 mg of **1** were mixed and ground together by an agate mortar and pestle to achieve a uniform mixture, and then was added to 0.1 mL of Nujol with stirring. The homogenized mixture was packed into a glass tube with a 1.5 mm inner diameter and the tube surface was wiped with paper. Electrical contact was established with a copper rod through the back of the electrode. In a similar manner, **2**-CPE was made with **2**.

3. Results and discussion

3.1. *Synthesis*

Under hydrothermal conditions, Cu^{II} in the POMs' system can usually be reduced by organonitrogen species [30] when the ratio of organonitrogen : Cu^{II} is high. In this

Table 1. Crystal data and structure refinements for **1** and **2**.

	1	**2**
Empirical formula	$C_{40}H_{64}Cu_5N_{24}O_{40}PW_{12}$	$C_{40}H_{64}Cu_2N_{24}O_{40}SiW_{12}$
Formula weight	4076	3882
Crystal system	Monoclinic	Monoclinic
Space group	$P2_1/c$	$P2_1/n$
Unit cell dimensions (Å, °)		
a	13.6234(9)	11.5359(9)
b	24.7644(1)	15.0948(12)
c	11.5519(7)	22.6817(19)
β	96.8360(1)	91.4830(10)
Volume (Å^3), Z	3869.6(4), 2	3948.3(6), 2
Calculated density (g·cm^{-3})	3.498	3.266
Absorption coefficient (mm^{-1})	19.215	18.04
$F(000)$	3680	3504
R_{int}	0.0467	0.0478
Goodness-of-fit on F^2	1.015	1.069
Final R indices [$I > 2\sigma(I)$]	$R_1{}^a = 0.0465$, $wR_2{}^b = 0.1128$	$R_1{}^a = 0.0677$, $wR_2{}^b = 0.1528$
R indices (all data)	$R_1{}^a = 0.0590$, $wR_2{}^b = 0.1210$	$R_1{}^a = 0.1073$, $wR_2{}^b = 0.1759$
Largest difference peak and hole (e Å^{-3})	2.610 and −2.879	3.877 and −4.205

[a] $R_1 = \sum|F_o| - |F_c|/\sum|F_o|$; [b] $wR_2 = \{\sum[w(F_o^2 - F_c^2)^2]/\sum[w(F_o^2)^2]\}^{1/2}$.

Table 2. The coordination environments of Keggin POMs, copper ions, and btx ligands in **1** and **2**.

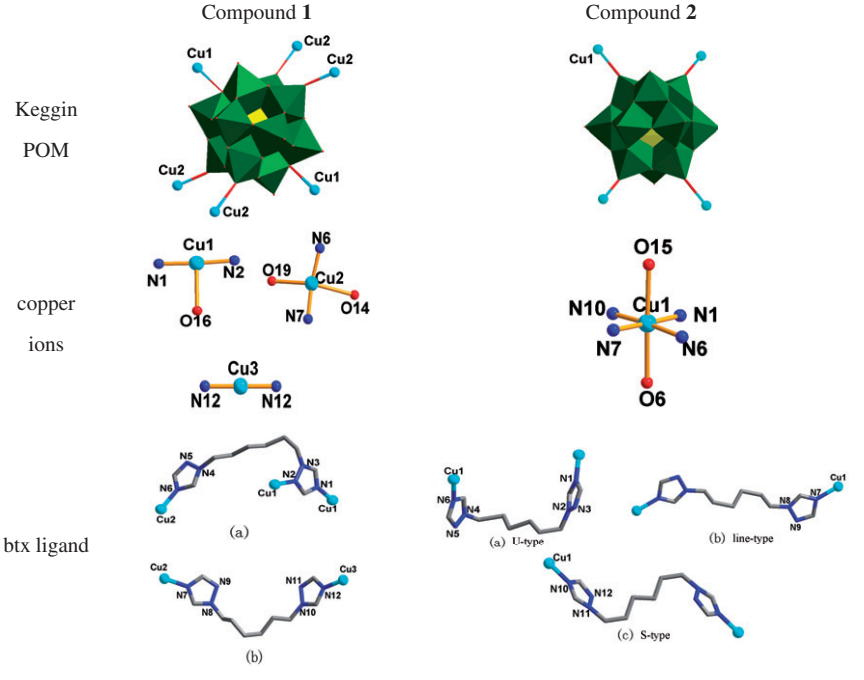

system, the organonitrogen species are ligands and reductants. Cu^I is usually insoluble in water, inhibiting formation of structures, but reduction under high ratio of organonitrogen : Cu^{II} provides a route to Cu^I as reactants. Fortunately, Cu^I ions were captured in **1** by increasing the ratio of btx : Cu^{II}.

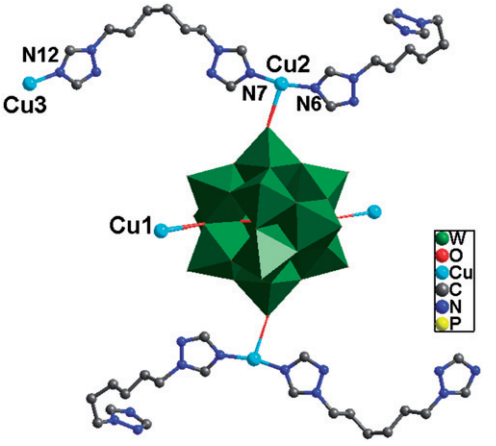

Figure 1. Ball/stick and polyhedral view of the asymmetric unit of **1**. Hydrogen atoms are omitted for clarity.

3.2. *Description of the structure*

$[Cu^{I}_{5}(btx)_4(PW^{VI}_{10}W^{V}_{2}O_{40})]$ (**1**). Crystal structure analysis reveals that **1** consists of five Cu^{I} ions, four btx ligands, and one $[PW^{VI}_{10}W^{V}_{2}O_{40})]^{5-}$ (abbreviated to PW_{12}) (figure 1). The PW_{12} shows a classical α-Keggin type anion, with P–O distances of 1.411(13)–1.666(8) Å, W–O_t 1.660(10)–1.690(8) Å, W–$O_{b/c}$ 1.876(9)–1.923(8) Å, and W–O_a, 2.337(13)–2.521(13) Å. Valence sum calculations [31] show that two out of twelve tungstens are +V oxidation state and all the coppers are in +I oxidation state.

In **1**, Cu^{I} ions show three coordination modes (table 2). Cu1 is three-coordinate by two nitrogen atoms from two btx, and one bridging oxygen atom from PW_{12} in a slightly distorted T-type coordination. The bond distances and angles around Cu1 are 1.889(8) and 1.895(10) Å for Cu–N, 2.581(4) Å for Cu–O, 171.3(5)° for N–Cu–N, and 90.27(3)–94.71° for N–Cu–O. Cu2 is four-coordinate by two nitrogen atoms from two btx and two terminal oxygen atoms from two PW_{12} in a "seesaw" geometry with Cu–N distances of 1.872(10) and 1.879(11) Å, Cu–O distances of 2.398(8) and 2.604(8) Å, Cu–N–Cu angle of 164.4(5)°, and N–Cu–O angles of 86.27(3)–101.59(3)°. Cu3 is linear, coordinated by two nitrogen atoms from two btx, with Cu–N distances of 1.880(12) Å and Cu–N–Cu angle of 180.0(2)°. These bond distances and angles are comparable to those in the two-, three-, and four-coordinated Cu^{I} compounds [32].

The btx in **1** exhibits two kinds of coordination modes (table 2). The N1-containing btx is an unsymmetrical tridentate ligand by offering three nitrogen donors to coordinate with three Cu^{I} ions. The N7-containing btx provides two apical N7 to link two Cu^{I} ions as a bidentate ligand. Furthermore, six N1-containing and four N7-containing btx are connected by ten Cu^{I} to build a decanuclear Cu^{I} circuit (figure S1). These circuits share N1-containing btx to construct a grid-like 2-D layer (figure 2a). Owing to the bend of N1-containing btx, there exists a channel of this layer along the *c*-axis (figure 2b). The large dimensions of the decanuclear Cu^{I} circuits allow three sets of these layers to interpenetrate to build a three-fold interpenetrating framework (figure 2c). The Keggin polyanions are six-connected inorganic linkages connecting

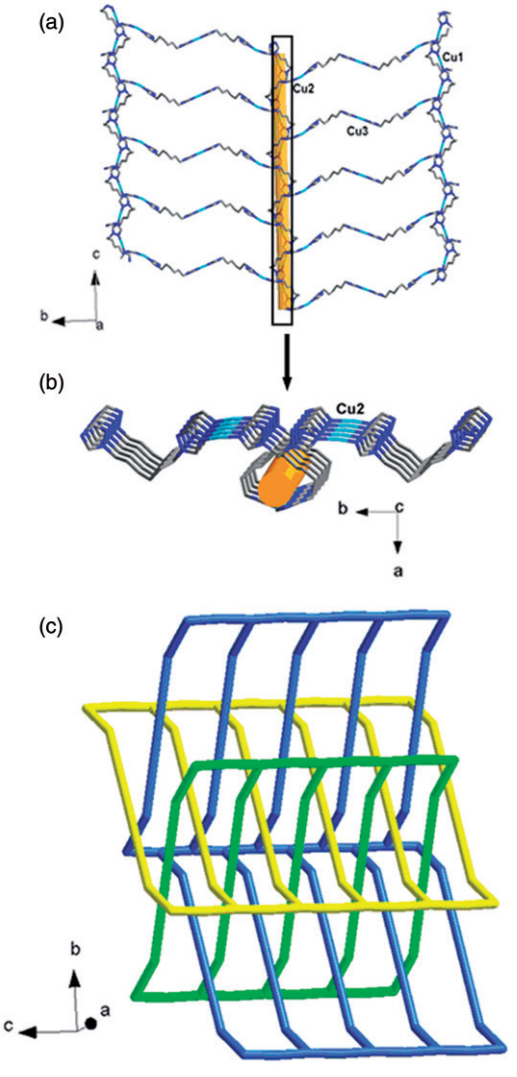

Figure 2. (a) The 2-D grid-like layer composed by decanuclear Cu^{I} circuits; (b) a channel of this 2-D layer exists along the *c*-axis; and (c) the three-fold interpenetrating structure in **1**.

adjacent three-fold interpenetrating frameworks to construct a 3-D structure by providing four terminal and two bridging oxygen atoms (figure 3).

$[Cu_2^{II}(btx)_4(SiW_{12}O_{40})]$ (**2**). Crystal structure analysis reveals that **2** consists of two Cu^{II} ions, four btx ligands, and one $[SiW_{12}O_{40})]^{4-}$ (abbreviated to SiW_{12}) anion (figure 4). The SiW_{12} shows a classical α-Keggin type anion with Si–O distances of 1.53(3)–1.73(3) Å, W–O_t 1.638(16)–1.672(15) Å, W–$O_{b/c}$ 1.83(2)–1.95(2) Å, and W–O_a 2.27(3)–2.49(2) Å. The valence sum calculations [31] show that all the tungstens are +VI and all coppers are +II.

Cu^{II} ion in **2** exhibits an octahedral coordination coordinated by four nitrogen atoms from four btx and two terminal oxygen atoms from two SiW_{12} anions (table 2).

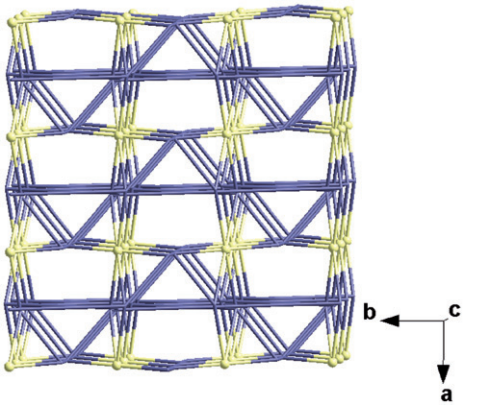

Figure 3. The 3-D framework of compound **1** containing interpenetrating layers (stick) linked by POMs (balls).

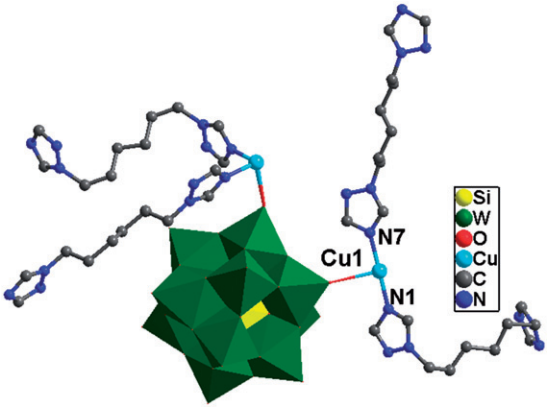

Figure 4. Ball/stick and polyhedral view of the asymmetric unit of **2**. Hydrogen atoms are omitted for clarity.

The bond distances and angles around Cu1 are 1.96(3)–2.06(2) Å for Cu–N, 2.54(5) and 2.62(3) Å for Cu–O, 88.9(11)–178.2(13)° for N–Cu–N, and 87.08(3)–94.77(4)° for N–Cu–O. The btx offers two apical N donors to link two Cu ions showing three coordination modes (table 2), U-type, linear, and S-type. Four U-type and two S-type btx ligands are linked by six Cu^{II} ions to form a hexanuclear circuit (figure S2). Adjacent hexanuclear circuits are further connected by linear ligands inducing a 1-D channel structure, as shown in figure 5. The 1-D channels share Cu^{II} ions to build a 3-D framework (Schläfli symbol: 6^6) with hexagonal channels (figure 6 (left)). The SiW_{12} anion provides four symmetrical terminal oxygen atoms to coordinate with Cu^{II} of the 3-D metal–organic framework (MOF) imbedding in the hexagonal channels (figure 6 (right)).

3.2.1. Influence of different oxidation states of the Cu ion (+I/+II) on their coordination geometries and the whole structure. As discussed above, Cu^{II} in POMs' systems can usually be reduced by organonitrogen species under hydrothermal conditions. In this

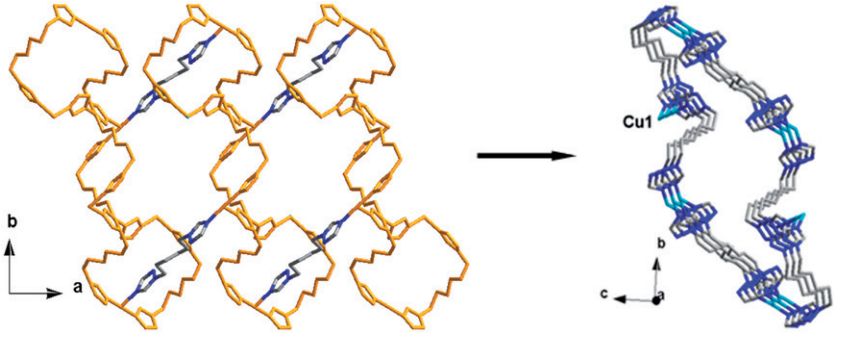

Figure 5. The hexa-nuclear circuits are connected by line-type ligands (left) to construct a 1-D channel structure (right).

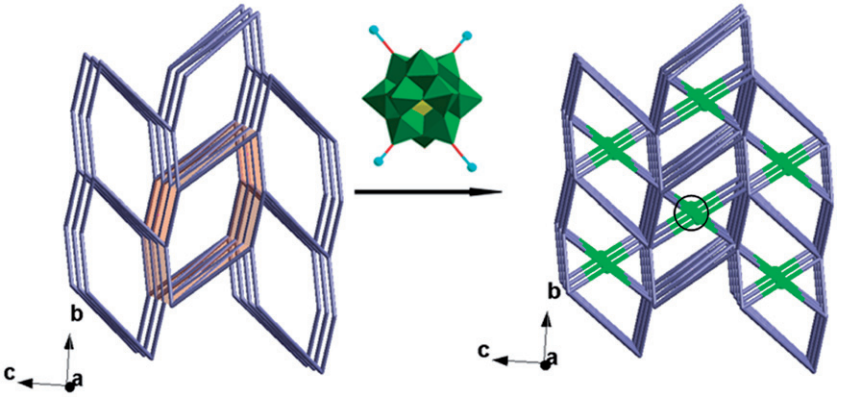

Figure 6. Left: The 3-D MOF with hexagonal channels in compound **2**; Right: The SiW_{12} anion acting as a four-connected linkage (in circle) embedding in the hexagonal channels.

work, when the ratio of organonitrogen : Cu^{II} was 1 : 5, Cu^{II} was reduced to Cu^{I} in **1**, while Cu^{II} in **2** was maintained with organonitrogen : Cu^{II} of 1 : 15. Different oxidation states of Cu ions (+I/+II) influence their coordination geometries (table 2) and the whole structures. In **1**, Cu^{I} ions show linear, T-type, and "seesaw" coordination modes. The coordination geometries of Cu^{I} may induce the high connectivity of PW_{12} anions and interesting coordination modes of btx. The PW_{12} anion offers four terminal and two bridging oxygen atoms as a six-connected inorganic linkage; btx exhibit symmetrical and unsymmetrical coordination to link two and three Cu^{I} ions, respectively. The coordination modes of Cu^{I} ions, btx, and anions induce three-fold interpenetrating MOFs, which are further linked by PW_{12} forming a 3-D structure of **1**. However, in **2** Cu^{II} only shows a single octahedral coordination. Owing to the Jahn–Teller effect, the octahedron is stretched containing two longer Cu–O bonds. The btx only is a bidentate ligand. Compound **2** contains a 3-D channel-like MOF with SiW_{12} anions imbedding in the hexagonal channels. Tuning the oxidation states of Cu ions is an effective strategy for construction of different Keggin-based topology structures.

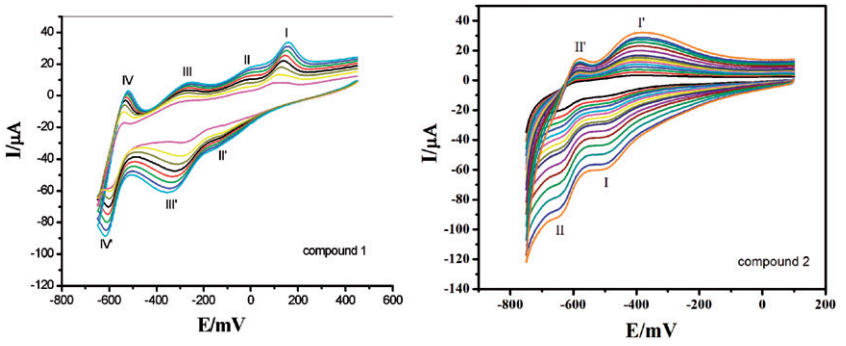

Figure 7. The cyclic voltammograms of **1**- and **2**-CPE in 1 molL^{-1} H_2SO_4 at different scan rates (from inner to outer: 40, 60, 80, 100, 120, 140, 160, and 180 mVs^{-1} for **1** and 40, 60, 80, 100, 120, 140, 160, 180, 200, 220, 240, 260, 280, 300, and 320 mVs^{-1} for **2**, respectively).

3.3. *IR spectra*

IR spectra of **1** and **2** are shown in figure S3. In **1**, characteristic bands at 962, 878, 795, and 1065 cm^{-1} are attributed to ν(W–O_t), ν(W–O_b–W), ν(W–O_c–W), and ν(P–O), respectively. In **2**, bands at 968, 923, 872, and 792 cm^{-1} are attributed to the ν(W–O_d), ν(Si–O), and ν(W–O_c–W) bands, respectively. Bands at 1654–1142 cm^{-1} for **1** and 1693–1124 cm^{-1} for **2** are attributed to btx.

3.4. *Thermogravimetric analyses*

TGA experiments were performed under N_2 with a heating rate of 10°C min^{-1} from 30°C to 800°C for **1** and **2** (figure S4). The TG curves of **1** exhibit one weight loss, ascribed to loss of btx 22.94% (calcd 21.98%). The TG curve of **2** shows two distinct weight loss steps corresponding to loss of btx 21.79% (calcd 22.69%).

3.5. *Cyclic voltammetry*

Due to the insolubility of **1** and **2**, the bulk-modified CPE becomes the optimal choice to study their electrochemical properties, inexpensive, and easy to prepare and handle [33].

Redox properties of **1** and **2** were studied in 1 mol L^{-1} H_2SO_4 aqueous solution (figure 7). The cyclic voltammograms for **1**-CPE at different scan rates are presented from −650 to +450 mV with three reversible redox peaks II–II′, III–III′, and IV–IV′ with half-wave potentials ($E_{1/2} = (E_{pa} + E_{pc})/2$) at −73 (II–II′), −297 (III–III′), and −565 (IV–IV′) mV (scan rate: 120 mV s^{-1}), respectively. Redox peaks II–II′, III–III′, and IV–IV′ correspond to three consecutive two-electron processes of PW_{12} [34]. The irreversible anodic peak I with the potential of +147 mV for **1**-CPE is assigned to oxidation of the copper [19]. In the potential range −750 to +100 mV for **2**-CPE, there exist two reversible redox peaks I–I′ and II–II′ with the half-wave potentials at −449 (I–I′) and −614 (II–II′) mV for **2**-CPE (scan rate: 100 mVs^{-1}). Redox peaks I–I′ and II–II′ correspond to two consecutive two-electron processes of SiW_{12} [28, 34].

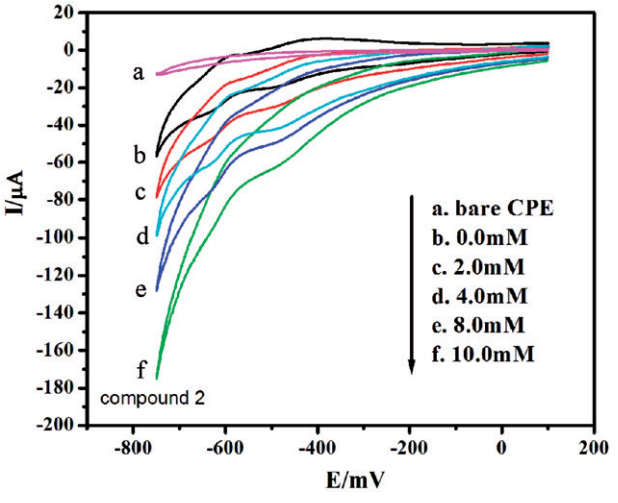

Figure 8. Cyclic voltammograms of a bare CPE (a) and the **2**-CPE in 1 mol L^{-1} H_2SO_4 containing 0 (b); 2 (c); 3 (d); 8 (e) 10.0 (f) m mol L^{-1} $NaNO_2$. Scan rate: 80 mV s^{-1}.

However, oxidation of copper is not observed in the scan range of −750 to +100 mV. This was also observed in $[Cu_2(bpp)_4(H_2O)_2](SiW_{12}O_{40}) \cdot 6H_2O$ [35]. As compared to reported PW_{12} and SiW_{12} systems, the slight potential shifts of the three and two redox peaks in **1**- and **2**-CPEs may relate to combination of Cu ligand complex cations. When scan rates varied from 40 mV s^{-1} to 180 mV s^{-1} for **1**-CPE and 40 to 320 mV s^{-1} for **2**-CPE, the peak potentials change gradually: the cathodic peak potentials shift toward the negative direction and the corresponding anodic peak potentials to the positive direction with increasing scan rates.

Figure 8 shows cyclic voltammograms for the electrocatalytic reduction of nitrite at **2**-CPE in 1 mol L^{-1} H_2SO_4 aqueous solution; **2**-CPE displays electrocatalytic activity toward the reduction of nitrite. At **2**-CPE, with the addition of nitrite, both reduction peak currents increase gradually while the corresponding oxidation peak currents gradually decrease, suggesting that nitrite is reduced by two- and four-electron reduced SiW_{12} anions. However, **1**-CPE has no obvious electrocatalytic reduction of nitrite in 1 mol L^{-1} H_2SO_4 aqueous solution.

4. Conclusion

Two new Keggin-based compounds have been obtained under hydrothermal conditions. Both are based on the Keggin–Cu–btx system with difference resting on the oxidation states of Cu ions, +I in **1**, and +II in **2**. The different oxidation states of Cu ions induce distinct topologies. In **1**, a 3-D framework containing three-fold interpenetrating MOFs is linked by Keggin anions. Compound **2** shows a 3-D hexagonal channel MOF with Keggin anions imbedding in the channels. Tuning the oxidation state of Cu is an effective strategy for construction of Keggin-based structures.

Supplementary material

CCDC 860727 for **1** and 860728 for **2** contain the supplementary crystallographic data for this article. These data can be obtained free of charge from The Cambridge Crystallographic Centre *via* www.ccdc.cam.ac.uk/data-request/cif.

Acknowledgments

We are grateful to the National Natural Science Foundation of China (Nos 21101015 and 21171025), New Century Excellent Talents in University (NCET-09-0853), and Doctoral Initiation Project of Liaoning Province (No. 20111147) for the financial support.

References

[1] Y. Hou, M. Nyman, M.A. Rodriguez. *Angew. Chem., Int. Ed.*, **50**, 12514 (2011).
[2] C. Zou, Z.J. Zhang, X. Xu, Q.H. Gong, J. Li, C.D. Wu. *J. Am. Chem. Soc.*, **134**, 87 (2012).
[3] D.Y. Du, J.S. Qin, Y.G. Li, S.L. Li, Y.Q. Lan, X.L. Wang, K.Z. Shao, Z.M. Su, E.B. Wang. *Chem. Commun.*, 2832 (2011).
[4] F.J. Ma, S.X. Liu, C.Y. Sun, D.D. Liang, G.J. Ren, F. Wei, Y.G. Chen, Z.M. Su. *J. Am. Chem. Soc.*, **133**, 4178 (2011).
[5] Y.L. Zhong, W. Ng, J.X. Yang, K.P. Loh. *J. Am. Chem. Soc.*, **131**, 18293 (2009).
[6] X.H. Yan, P.L. Zhu, J.B. Fei, J.B. Li. *Adv. Mater.*, **22**, 1283 (2010).
[7] S.T. Zheng, J. Zhang, X.X. Li, W.H. Fang, G.Y. Yang. *J. Am. Chem. Soc.*, **132**, 15102 (2010).
[8] H. Liu, C. Qin, Y.G. Wei, L. Xu, G.G. Gao, F.Y. Li, X.S. Qu. *Inorg. Chem.*, **47**, 4166 (2008).
[9] H.S. Liu, C.J. Gómez-García, J. Peng, Y.H. Feng, Z.M. Su, J.Q. Sha, L.X. Wang. *Inorg. Chem.*, **46**, 10041 (2007).
[10] S.T. Zheng, J. Zhang, J.M. Clemente-Juan, D.Q. Yuan, G.Y. Yang. *Angew. Chem., Int. Ed.*, **48**, 7176 (2009).
[11] X.L. Wang, C. Qin, E.B. Wang, Z.M. Su, Y.G. Li, L. Xu. *Angew. Chem., Int. Ed.*, **45**, 7411 (2006).
[12] X.L. Wang, Y.F. Bi, B.K. Chen, H.Y. Lin, G.C. Liu. *Inorg. Chem.*, **47**, 2442 (2008).
[13] Y.Q. Lan, S.L. Li, X.L. Wang, K.Z. Shao, D.Y. Du, Z.M. Su, E.B. Wang. *Chem. Eur. J.*, **14**, 9999 (2008).
[14] M.L. Wei, H.H. Li, G.J. He. *J. Coord. Chem.*, **64**, 4318 (2011).
[15] P. Shringarpure, B.K. Tripuramallu, K. Patel, A. Patel. *J. Coord. Chem.*, **64**, 4016 (2011).
[16] Q.J. Kong, M.X. Hu, Y.G. Chen. *J. Coord. Chem.*, **64**, 3237 (2011).
[17] M.L. Wei, P.F. Zhuang, R.P. Sun. *J. Coord. Chem.*, **63**, 3384 (2010).
[18] H.N. Chen, Q. Wu, J.W. Zhao, S.Z. Li, J.P. Wang, J.Y. Niu. *J. Coord. Chem.*, **63**, 1463 (2010).
[19] A.X. Tian, J. Ying, J. Peng, J.Q. Sha, Z.G. Han, J.F. Ma, Z.M. Su, N.H. Hu, H.Q. Jia. *Inorg. Chem.*, **47**, 3274 (2008).
[20] L. Lisnard, A. Dolbecq, P. Mialane, J. Marrot, E. Codjovi, F. Sécheressea. *Dalton Trans.*, **34**, 3913 (2005).
[21] J.Q. Sha, J. Peng, H.S. Liu, J. Chen, B.X. Dong, A.X. Tian, Z.M. Su. *Eur. J. Inorg. Chem.*, 1268 (2007).
[22] C. Qin, X.L. Wang, E.B. Wang, Z.M. Su. *Inorg. Chem.*, **47**, 5555 (2008).
[23] H.J. Pang, J. Peng, C.J. Zhang, Y.G. Li, P.P. Zhang, H.Y. Ma, Z.M. Su. *Chem. Commun.*, 5097 (2010).
[24] X.L. Wang, H.L. Hu, G.C. Liu, H.Y. Lin, A.X. Tian. *Chem. Commun.*, 6485 (2010).
[25] Y.Q. Lan, S.L. Li, X.L. Wang, K.Z. Shao, Z.M. Su, E.B. Wang. *Inorg. Chem.*, **47**, 529 (2008).
[26] K. Pavani, S.E. Lofland, K.V. Ramanujachary, A. Ramanan. *Eur. J. Inorg. Chem.*, 568 (2007).
[27] J.Q. Sha, J. Peng, Y.Q. Lan, Z.M. Su, H.J. Pang, A.X. Tian, P.P. Zhang, M. Zhu. *Inorg. Chem.*, **47**, 5145 (2008).
[28] A.X. Tian, J. Ying, J. Peng, J.Q. Sha, H.J. Pang, P.P. Zhang, Y. Chen, M. Zhu, Z.M. Su. *Inorg. Chem.*, **48**, 100 (2009).
[29] G.M. Sheldrick. *Acta Crystallogr. A*, **64**, 112 (2008).

[30] C.M. Liu, D.Q. Zhang, D.B. Zhu. *Cryst. Growth Des.*, **6**, 524 (2006).
[31] I.D. Brown, D. Altermatt. *Acta Crystallogr. B*, **41**, 244 (1985).
[32] H.Y. Liu, H. Wu, J.F. Ma, Y.Y. Liu, J. Yang, J.C. Ma. *Dalton Trans.*, **40**, 602 (2011).
[33] Z.G. Han, Y.L. Zhao, J. Peng, Q. Liu, E.B. Wang. *Electrochim. Acta*, **51**, 218 (2005).
[34] M. Sadakane, E. Steckhan. *Chem. Rev.*, **98**, 219 (1998).
[35] X.L. Wang, H.Y. Lin, Y.F. Bi, B.K. Chen, G.C. Liu. *J. Solid State Chem.*, **181**, 556 (2008).